Sensors & Transducers, Vol. 204, Issue 9, September 2016, pp. 11-20

Sensors & Transducers

http://www.sensorsportal.com

A New Approach to Eliminate High Amplitude Artifacts in EEG Signals

[1] Ana Rita Teixeira, [2] Ana Maria Tomé, [3] Isabel Maria Santos

[1] University of Aveiro / IEETA, Aveiro, Portugal and IPC/ ESEC 3030-329 Coimbra, Portugal
[2] University of Aveiro DETI/IEETA, 3810-193 Aveiro, Portugal
[3] University of Aveiro, Department of Education and Psychology/
CINTESIS 3810-193 Aveiro, Portugal
[1] Tel.: (+351) 234 370 200, fax: (+351) 234 370 985
[1] E-mail: ateixeira@ua.pt

Received: 4 July 2016 /Accepted: 31 August 2016 /Published: 30 September 2016

Abstract: High amplitude artifacts represent a problem during EEG recordings in neuroscience research. Taking this into account, this paper proposes a method to identify high amplitude artifacts with no requirement for visual inspection, electrooscillogram (EOG) reference channel or user assigned parameters. A potential solution to the high amplitude artifacts (HAA) elimination is presented based on blind source separation methods. The assumption underlying the selection of components is that HAA are independent of the EEG signal and different HAA can be generated during the EEG recordings. Therefore, the number of components related to HAA is variable and depends on the processed signal, which means that the method is adaptable to the input signal.

The results show, when removing the HAA artifacts, the delta band is distorted but all the other frequency bands are preserved.

A case study with EEG signals recorded while participants performed on the Halstead Category Test (HCT) is presented. After HAA removal, data analysis revealed, as expected, an error-related frontal ERP wave: the feedback-related negativity (FRN) in response to feedback stimuli. *Copyright © 2016 IFSA Publishing, S. L.*

Keywords: BSS, EEG, ERP, FRN, Source Selection.

1. Introduction

The electroencephalogram (EEG) signals measured by placing electrodes over the scalp represent the bioelectrical brain activity which may be used, amongst different applications, in neuroscience studies. During the recordings, the EEG signal is, unfortunately, often contaminated with different biophysical signals independent of the cerebral activity which are typically not of interest - commonly called artifacts. The elimination of artifacts is an important issue in EEG signal processing and is in many studies a prerequisite to achieve reliable signal analysis in the following processing steps.

For instance, in Brain Computer Interfaces applications, where EEG features are used to control devices, the feature values are clearly degraded with the presence of artifacts [1]. There are several EEG waveforms that differ from background EEG rhythms and may be of interest for particular research and clinical assessment aims. A relevant type of waveform that is studied independently from background EEG activity is the event-related potential. ERPs are deterministic signals, i.e they are evoked and not spontaneous like the rhythms. ERPs are a transient form of brain activity generated in the brain structures in response and time-locked to specific events or stimuli. Recent studies show that ERP waves can be

used for non-muscular BCI control [2]. There are advantages and drawbacks of using ERPs in BCI. The two main advantages are that 1) ERPs are responses, which the user produces without any particular training; 2) ERPs occur at short latencies, which is a beneficial property for the throughput of a BCI. However, these advantages are counterbalanced by some drawbacks. Firstly there are large inter-individual differences in ERP latencies and waveforms, requiring the system to be trained to recognize the ERP of a given individual. Another drawback is that ERP waves have small amplitudes and are dominated by background activity, which makes them difficult to detect to the human eye. Several methods exist to extract the ERP signal from the EEG background. Simple Fsignal processing techniques including averaging over consecutive trials can reveal their shape and allow their analysis if the EEG signal is not corrupted by artifacts, mainly high amplitude artifacts. The common high amplitude artifacts are eye blinks, eye movements and patient movements which affect the scalp electrodes differently. However, the frontal channels are specially affected by this kind of artifacts, in particular by the ocular artifacts. Furthermore, it can be verified that the temporal correlation values between artifacts and frontal channels are large while the temporal correlation values between artifact and non-frontal channels is not so large. In summary the high amplitude artifact correction can be regarded as a preprocessing step to clean the EEG signal. There are three main ways of dealing with high amplitude artifacts.

1) Prevention:

Minimize the occurrence of ocular artifacts and patient movements by giving proper instructions to patients. However, it is often impossible to prevent the appearance of blinks, since they are spontaneous, involuntary and often task dependent.

2) Epoch Rejection:

Manual Method: This is a very simple method to eliminate the artifacts in EEG signal. If an artifact exists then the corrupted epoch is removed. However, in that way, important data can be lost, and if a high number of trials needs to be removed, all the experiment is compromised.

3) Elimination of artifacts:

Different denoising techniques can be used to eliminate artifacts from the EEG signal. This is the best approach for cleaning the EEG because the number of epochs is preserved.

Blind Source Separation (BSS) techniques are nowadays a standard way to achieve noise reduction and artifact removal [3]. Actually BSS algorithms investigate several alternatives and even more promising approaches [4]. The goals are not only to reduce the noise, but also to enhance some brain patterns and to improve the sources localization. In that way, the spatial resolution of the brain, as well as interpretation of the features are achieved [5].

In summary, the application of BSS methods, namely Independent Component Analysis (ICA) to eliminate artifacts, has the advantage of not being dependent on reference signals but, instead the artifact related components need to be identified. One disadvantage of ICA, along with other BSS techniques, is knowing how to identify the components related to the artifacts. However, ICA methods suffer from amplitude and order inderminancies. Therefore, after an ICA decomposition, it is necessary to identify the component related artifacts [6].

The identification of artifact related components among the components of an ICA decomposition mostly assume that the components have some special characteristics. Some works assume that artifacts have peak values larger than a threshold [7, 8]; or take into account the kurtosis of the component [9], or the mutual information estimated on component distribution [7], and finally others measure spectral properties [7]. But the variability of the values of referred features does not allow identifying component as artifact or neural signal via the definition of simple thresholds. Therefore, most of the available tools are designed to assist experimented users to select the components. For instance, different EEGLAB (a MATLAB toolbox used to process EEG and ERP signals) plug-ins such as ADJUST [10], FASTER [11] and AAR [9] and SASICA [12] follow this trend. Another problem to face is the existence of many alternatives to perform ICA decompositions. Several works can be found which try to compare the different ICA algorithms [13, 8, 7]. But the lack of ground-true signals in order to have a quantitative measure to evaluate possible distortions does not allow to achieve a universal conclusion. Therefore, experimental studies with artificially mixed signals were conducted [14, 15] trying to overcome the ground-truth problem. Other works use non-direct measures of performance, for instance in [7] all correction methods are turned into detection methods by, once again, subtracting the corrected EEG signal from the raw EEG signal and thresholding the result. With the resulting binary signal, it is possible to mark zones with and without ocular artifacts. Short segments of the original signal are manually marked as artifact and non-artifact and the comparison with binary signal leads to definition of the detection performance measures to compare the algorithms. In spite of the reported drawbacks new EEG based applications need to apply artifact removal techniques. And the final decision about the effectiveness is once again dependent on the particular application. For instance in [16] the ICs are correlated with auxiliary accelerometer signal in order to identify movement related components.

The component selection method proposed in this work is based on the correlation coefficient index (CBI) [17] and on frontocentral topographic scalp distribution [18]. Such approach is able to identify high amplitude artifacts in a fully automatic way without requiring visual inspection, the EOG reference channel or free parameters as input [19]. This study presents a potential solution to the

elimination of high amplitude artifacts (HAA). The assumption underlying the selection method is that HAA are independent of the EEG signal and different HAA can be generated during the EEG recordings. Therefore the number of components related to HAA is variable and dependent on the processed signal, which means that the method is adaptive to the signal. The proposed method reduces the influence of high amplitude artifacts and improves the quality of the EEG signal allowing to find different ERP waves. It has been established for years that the brain produces specific event-related responses in case of errors. Along that line, a couple of recent studies have proposed to use error-related brain signals in BCI applications, [20]. The use of Error Potentials in BCI arises from the observation that this additional information provided automatically by the user could be used to improve the BCI performance, [21]. An example of such ERP waves is a large negative peak, the feedback-related negativity (FRN), observed in fronto-central electrodes [22]. The FRN is more pronounced when the feedback does not conform to the user's expectations after the feedback stimuli, thus being typically larger for incorrect than correct responses. Source estimation studies have localized the most likely neural generator of the FRN in the dorsal area of the anterior circulate cortex (ACC) [23].

In the present work, the preprocessing data analysis described allowed the visualization of an FRN wave during performance on the Halstead Category Test (HCT), which is a neuropsychological test that assesses a person's ability to formulate and apply abstract principles. During performance on the test, a person is required to adjust their response strategy based on feedback regarding the correctness of the previous response. Thus, a larger FRN is elicited by errors than correct responses, as expected [24]. Therefore, this preprocessing method shows potential to be used in improving the quality of the EEG signal used in neuroscience studies. Accordingly, this represents an effective solution to distinguish high amplitude artifact components automatically, easily, and accurately during a single acquisition. In particular the results can be useful in BCI applications to clean high amplitude artifacts as well as for the detection of FRN waves.

The remainder of this paper is organized as follows: Section 2 reviews blind source separation methodology and Section 3 describes the source selection methodology. The results are presented in Section 4, and in Section 5 some metrics for algorithm validation are discussed. Section 6 presents a case study based on ERP signals. Concluding remarks are provided in Section 7.

2. Blind Source Separation

The effectiveness of the BSS technique depends on some assumptions, according to the studied problem, such as: independence, linearity, uncorrelatedness, non-gaussianity, among others described in the literature. The more closely the hypotheses advanced by a certain algorithm are satisfied, the better the method is meant to separate the components. Success hence critically depends on good source separation and on correct identification of sources as brain activity or artifact components. In the literature, BSS is considered to be the best approach for artifacts of high signal to noise ratio (SNR), i.e., high amplitude artifacts [25]. Linear Blind Source Separation models can be expressed algebraically as

$$\mathbf{X} = \mathbf{AS}, \tag{1}$$

where the sensored EEG data is organized into a $C \times N$ matrix $\mathbf{X}$, representing C the number of channels and N the number of time points; $\mathbf{A}$ is the $C \times C$ mixing matrix and $\mathbf{S}$ is a $C \times N$ matrix of unknown sources or independent components. The goal of BSS or ICA algorithms is to determine the sources and the separation matrix $\mathbf{B}$ given the measured/ sensored signals $\mathbf{X}$. So, the separation equation reads

$$\mathbf{S} = \mathbf{BX}, \tag{2}$$

where $\mathbf{B}$ can be defined as the pseudo-inverse of the mixing matrix, i.e., $\mathbf{B} = \mathbf{A}^{\dagger}$.

Most of BSS/ICA algorithms follow a two step procedure to estimate the separation (or de-mixing) matrix [13]. The first step is based on Principal Component Analysis or Singular Value Decomposition (SVD) of the data matrix $\mathbf{X}$ [26]. For the second step different approaches have been proposed [26]. The separation matrix $\mathbf{B}$ is estimated as the product of matrices computed in both steps. For convenience, these steps are reviewed for the Second Order Blind Identification (SOBI) [27].

- With the SVD of the original data $\mathbf{X}$, two $C \times C$ matrices are computed: the eigenvector matrix $\mathbf{V}$ and the diagonal singular value matrix $\mathbf{D}$. Note that a dimension reduction can be performed by reducing the number of singular values and eigenvectors in the corresponding matrices.

- After whitening the original data, i.e., $\mathbf{Z} = \mathbf{D}^{-1}\mathbf{V}^{T}\mathbf{X}$, L time-delayed correlation matrices are estimated. The approximate joint diagonalization of these sets of matrices gives an orthogonal matrix $\mathbf{U}$.

The separation matrix is defined as $\mathbf{B} = \mathbf{U}^{T}\mathbf{D}^{-1}\mathbf{V}^{T}$ and its pseudo-inverse as $\mathbf{A} = \mathbf{VDU}$. The mandatory parameter of this algorithm is L, the number of matrices of second step. Eventually, the user can decide to perform dimension reduction after the first step by discarding the smallest singular values and corresponding eigenvectors. In this work, the dimension was maintained equal to the number of sensors (channels),

i. e. C, and the L is assigned to 100 and the default value of the energy of the components, i.e., the rows of the matrix $\mathbf{S}$, is equal to one. Therefore, the coefficients of the mixing matrix can be used to decide the relevance of the sources in the respective linearly mixed signal. It is also to be noticed that the columns of the mixing matrix are related to the scalp positions of the sensors.

3. Source Selection

Source selection, in BSS applications, is the problem most widely reported in the literature [13]. Existing methods for artifact rejection can be separated into hand-optimized, semiautomatic and fully automatic approaches. Semi-automatic approaches require user interaction for ambiguous or outlier components, while fully automated methods were proposed for the classification of artifacts. Whichever is the case, different metrics have been applied directly to the mixing matrix $\mathbf{A}$ or to the sources $\mathbf{S}$ in order to select artifact related components. In this study, as the sources have energy one, the columns of the mixing matrix determine the power distribution of the reconstructed sources over the scalp. Given, the mixing matrix $\mathbf{A}$

$$\mathbf{A} = \begin{pmatrix} a_{11} & a_{12} & \dots & a_{1C} \\ a_{21} & a_{22} & \dots & a_{2C} \\ \dots & \dots & & \dots \\ a_{C1} & a_{C2} & \dots & a_{CC} \end{pmatrix}, \quad (3)$$

where $a_{ij}, (1 \le i, j \le C)$ is the transfer coefficient from the $j-th$ source to the $i-th$ observed channel signal. Each column vector of the matrix **A** reflects the power propagating across all scalp channels of the corresponding row of **S** (one source). In this work a two-step fully automatic source selection procedure is proposed. The first step measures the influence, over the whole scalp, of each source by estimating the following coefficient

$$\theta(j) = \sum_{i=1}^{C} \frac{|a_{ij}|}{\sqrt{a_{i1}^2 + a_{i2}^2 + \dots + a_{iC}^2}} \quad (4)$$

Experimentally it was verified that the plot of θ values, ordered by decreasing order of magnitude, shows an abrupt decrease on the first five values and then stabilizes. So, the five largest θ values are initially identified as candidate columns of the matrix $\mathbf{A}$ associated to the high amplitude artifacts. For the sake of simplicity, from now on, we assume that the columns of **A** and the rows of **S** are ordered according to the values of the coefficient θ. Re-writing the mixing model as a sum of outer products

$$\tilde{\mathbf{X}} = \mathbf{AS} = \mathbf{A}_{*1}\mathbf{S}_{1*} + \mathbf{A}_{*2}\mathbf{S}_{2*} + \dots + \mathbf{A}_{*C}\mathbf{S}_{C*}, \quad (5)$$

where the first term ($\mathbf{A}_{*1}\mathbf{S}_{1*}$) on the right side of the equation 5 corresponds to the source spreading, over the scalp, with largest energy; the second term ($\mathbf{A}_{*2}\mathbf{S}_{2*}$) corresponds to the source spreading with the second largest energy and so on. As referred before, the graphical representation of the columns of $\mathbf{A}$ is often used by experts to visually identify the artifacts. The second step of the selection procedure is the application of one of the rules used in this context. To find out if a certain source is an artifact related component it is foreseen that it contributes mostly in the frontal region. To confirm if the five selected candidate columns with highest θ are related to the high amplitude artifact, the power distribution for all selected j columns should verify the condition:

- $|a_{ij}| > |a_{kj}|$, $\forall i \in L_1$ and $k \in L_2$,

where

- $L_1 = [Fp1; Fpz; Fp2]$,
- $L_2 = [F7; F3; Fz; F4; F8]$.

Note that after the selection of the artifact related sources the original signal is decomposed into the artifact related signal and the clean signal. The reconstructed signal is then obtained without high amplitude artifacts. By the explanation above it is clear that the EEG signal can be expressed as:

$$\mathbf{X} = (\mathbf{A_1} + \mathbf{A_2})\mathbf{S}, \quad (6)$$

where $\mathbf{A_1}$ $(C \times C)$ is the matrix with columns associated to the EEG activity (Clean Data) and $\mathbf{A_2}$ $(C \times C)$ is the matrix with $j \le 5$ non null columns associated to the high amplitude artifacts activity (HAA Data).

4. Experimental Procedure

The following subsections describe the participants, the task and the dataset. The algorithm performance is discussed in the last subsection considering a trial without artifacts (Case 1) and a trial corrupted with HAA artifacts (Case 2).

4.1. Participants and Task

Fifty eight EEG signals belonging to 58 participants with 208 trials each were collected with a Neuroscan SynAmps2 amplifier through an Easy-Cap with 26 channels and recorded with the software Scan 4.3 (Neuroscan Systems). EEG was continuously recorded at 1000 Hz with Ag-AgCl

sintered electrodes which were located according to the 10 - 20 system. A computerized version of the Halstead Category Test (HCT) was used to assess cognitive executive frontal lobe function. The HCT is a well-established neuropsychological measure of non-verbal reasoning, abstract concept formation and cognitive flexibility, which are aspects of the cognitive executive function.

This test is used to measure a person's ability to formulate abstract principles based on receiving feedback after each specific test item. Visual feedback is provided after each trial, to indicate if the participant responded wrong or right [28].

4.2. Dataset

For signal analysis, each EEG trial was epoched from 6000 *ms* prior to response onset to 3000 *ms* after, leading to a dataset with 208 trials for each of the 58 participants. Note that after 1500 *ms* of response onset the feedback was provided and the dataset for each participant can be divided considering the conditions wrong and right response.

In this study, the Raw Data signal is the filtered EEG between [1 - 40] Hz in frequency, trial by trial, for each participant; the Clean Data signal is the processed Raw Data by SOBI algorithm with full automatic criteria to select the sources associated with the high amplitude artifacts; and the HAA Data is the reconstructed signal with the automatically rejected sources.

4.3. Algorithm Performance

As mentioned above, the SOBI algorithm is employed to decompose all epochs into two datasets: Clean and HAA Data. The selection of components is fully automatic, adaptable to each epoch allowing the identification of HAA signal. The number of selected components is variable between 0 and 5. Although almost all epochs in the present dataset were corrupted with high amplitude artifacts, there were occasionally epochs without artifacts. In epochs without artifacts, no components are selected. In these datasets ≈ 97 % of the trials were corrupted with artifacts and the number of selected components in all trials was in average 1.85±0.98. To demonstrate the algorithm performance two distinct cases are discussed: Case 1 - An epoch without artifacts, and Case 2 - An epoch with artifacts.

4.3.1. Case 1: Epoch without Artifact

Fig. 1 (a) represents an example of an epoch without artifact (only 1 second is represented). In this case, the automatic algorithm did not select any component. Considering the maximum peak of the channel *Fp1*, an average head topography centered in the *100 ms* window around the peak was constructed, Fig. 1(b), to illustrate that there are no high-amplitude components in this epoch.

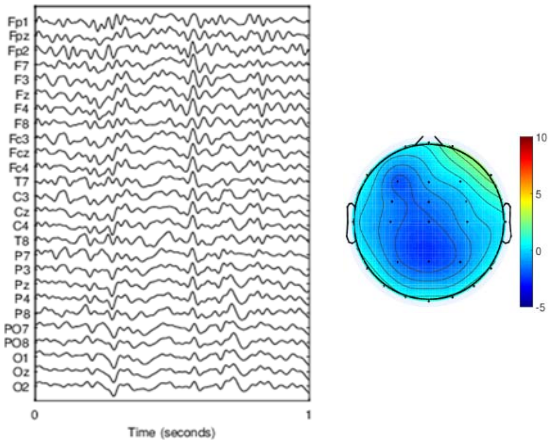

(a) Raw Data (b) Topogram of the Raw Data

Fig. 1. Case 1: (a) Original Epoch - Raw Data (b) Head topography of the corresponding Raw Data considering an average window of *100 ms* centered in maximum peak of the *Fp1* channel.

4.3.2. Case 2: Epoch with Artifact

In Fig. 2(a) is represented an example of an epoch with an artifact and Fig. 2(b) represents clean data after the HAA were removed by the automatic proposed method (only 1 second is represented). In this case, the algorithm selected 4 components (S_{*1}, S_{*3}, S_{*4} and S_{*5}) of the 5 with the largest spread on the scalp. As shown in the head topographies, Fig. 2(c), all components selected by the algorithm have a strong power energy in frontal channels. It should be noted that, although the first component (S_{*1}) has the highest energy in the frontal channels, the selection of only this component is not sufficient to remove the HAA signal, as described in [17].

5. Metrics for Algorithm Validation

The automatic selection of the components' efficiency was validated using different metrics to compare the Raw Data, the Clean Data and the HAA Data in time and frequency domains in each epoch for all participants. Firstly, the datasets (Raw, Clean and HAA signals) were grouped according to the region of the scalp where the electrodes were located. To account for spatial differences in amplitude distribution, channels were grouped into 6 regions, as represented in Fig. 3.

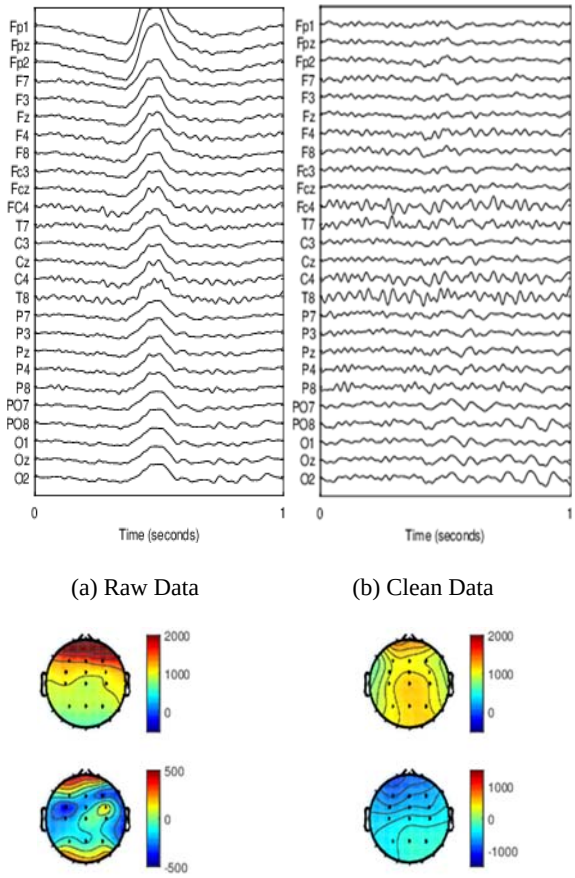

(a) Raw Data (b) Clean Data

(c) Topograms of the selected IC's related with artifacts

Fig. 2. Case 2: (a) Original Epoch - Raw Data (b) Clean Data after HAA signal removed by the automatic proposed method to select the ICs (c) Head topography of the selected ICs associated to HAA signal.

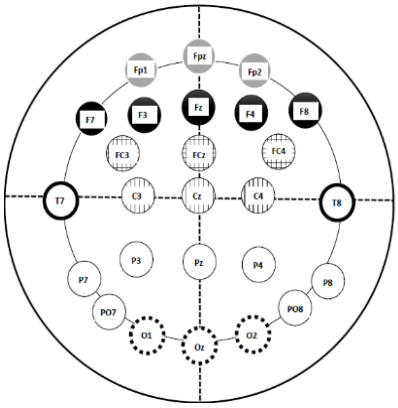

Fig. 3. Montage 10-20 system. The scalp is divided into 6 regions: Prefrontal; Frontal; Frontocentral; Parietal; Parieto-occipital and Temporal.

Regions:

R1: prefrontal channels *(Fp1, Fp2, Fpz),*

R2: frontal channels *(F7, F3, Fz, F4, F8),*

R3: frontocentral channels *(FC3, FCz,FC4, C3, Cz, C4),*

R4: parietal channels *(P7, P3, Pz, P4, P8)*,

R5: parieto-occipital channels *(PO7, PO8, O1, Oz, O2)*,

R6: temporal channels *(T7, T8)*.

The three datasets in each region *(R1-R6)* were band-pass filtered (*6th* order Butterworth), with a zero-phase strategy, into delta: [1 - 4] Hz; theta: [4 - 7] Hz; alpha: [7 - 13] Hz and beta: [13 - 30] frequency bands. For all epochs and for all participants, the following metrics were then calculated per band in each region and were performed in three ways:

1) Correlation coefficient [29] in time for all signals:

$$\rho_{xy} = \frac{1}{N-1}\sum_{n=1}^{N}\left(\frac{x(n)-\mu_x}{\sigma_x}\right)\left(\frac{y(n)-\mu_y}{\sigma_y}\right), \quad (7)$$

where N is the number of time points *N=1:9000*, x and y represent the signals (Clean/Raw data; Clean/HAA Data and Raw/HAA Data) for each participant, μ_x, μ_y represents the mean and σ_x, σ_y the standard deviation of the signals x and y, respectively.

2) Relative power between the Clean and Raw Data:

$$RP = \frac{\sum_{i=1}^{I}\sum_{n=1}^{N} x_{c_i}(n)^2}{\sum_{i=1}^{I}\sum_{n=1}^{N} x_{r_i}(n)^2}, \quad (8)$$

where I represents the number of participants *i=1:58*, x_{c_i} is the Clean Data and x_{r_i} is the Raw Data in each band computed for each region and for all participants.

3) Magnitude-squared coherence [29] of grand average signals:

$$C_{xy}(f) = \frac{\left|P_{xy}(f)\right|^2}{P_{xx}(f)P_{yy}(f)} \quad (9)$$

where $P_{xx}(f)$ and $P_{yy}(f)$ are the power spectral density of the signals x and y (Clean/Raw data and Raw/HAA Data) and $P_{xy}(f)$ is the cross power spectral density.

The correlation coefficient was calculated between the Clean/HAA Data, the Raw/HAA Data and the Clean/Raw Data in each band for all regions, as shown in Fig. 4(a), (b) and (c) respectively. The results show that the Clean/Raw Data in *R3, R4, R5* and *R6* have a high correlation in beta, alpha and theta bands and, in turn, Raw/HAA Data presents high correlation in the delta band.

The correlation coefficient between the Clean/HAA data in each band for all regions is less than 0.5. Regions *R1* and *R2* are more affected by the HAA elimination and because of this, the correlation coefficient between the Clean/HAA Data in these regions presents lower correlations. The correlation coefficient between Raw/HAA data is high in delta

band in all regions. Furthermore, it is important to note that the correlation between Raw/HAA data in *R1* (region related to prefrontal channels) is high in all frequency bands. In addition, the correlation between Clean/Raw Data in the region R1 is small for all bands. Thus, it is possible to conclude that the proposed method reduces the influence of signals associated to the delta band namely high amplitude artifacts present in *R1*.

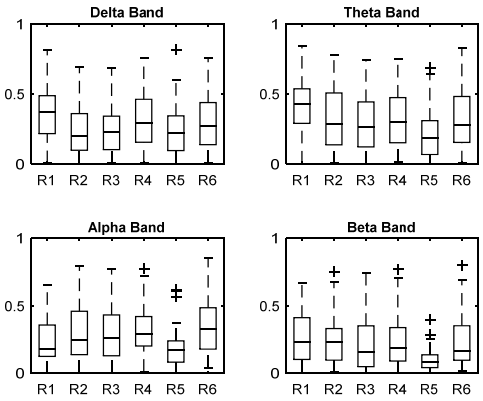

(a) Clean/ HAA data

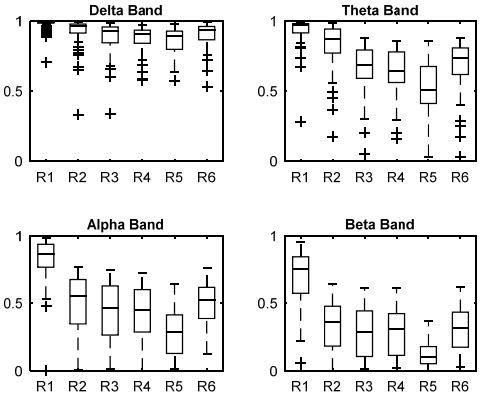

(b) Raw/HAA Data

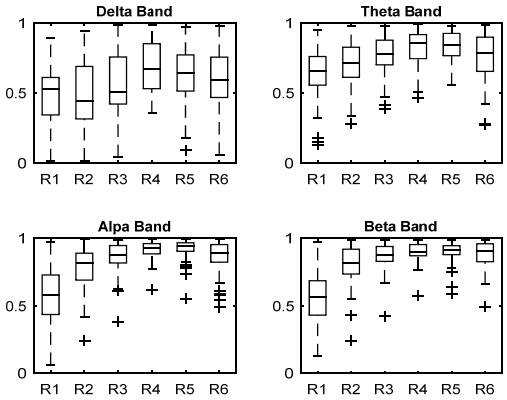

(c) Clean/Raw Data

Fig. 4. Correlation Coefficients between (a) – Clean/HAA Data; (b) - Raw/HAA Data; (c) – Clean/Raw Data in each band (delta, theta, alpha and beta) for each region (*R1, R2, R3, R4, R5* e *R6*).

To measure the relation in each band between the Clean and Raw Data in each band, the relative energy power *(RP)* for each region was computed. The results are consistent with the results described above considering the different metrics. The relative power between Clean/Raw Data in region *R3* is presented in Fig. 5. Once again, it can be seen that the band with greater loss of information is the delta band with some 40 % and that the alpha and beta bands exhibit residual losses, ≈ 10 %.

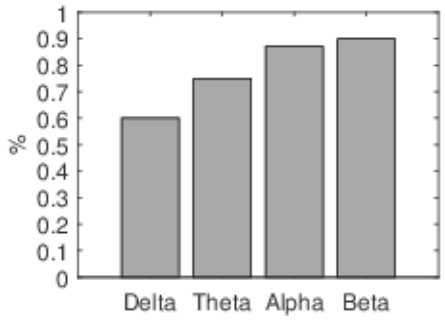

Fig. 5. Relative Power between Clean/Raw Data in region *R3*.

Fig. 6 presents the results of the computation of the magnitude squared coherence between the Raw/Clean Data and Raw/HAA Data in regions *R1, R2 R3* and *R5.* Coherence is a function of frequency with values between 0 and 1 that indicate how well two signals are similar at each frequency.

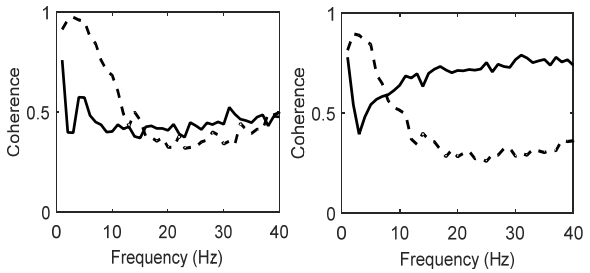

(a) R1 (b) R2

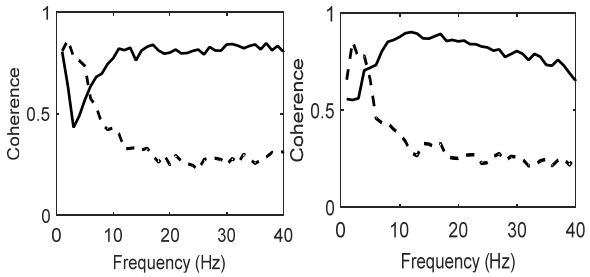

(c) R3 (d) R5

Fig. 6. Coherence Magnitude of the grand average signals, in regions *R1* (a), *R2* (b), *R3* (c) and *R5* (d) between the Raw/Clean Data (dash line) and between Raw/HAA Data (solid line).

Region *R1* is the most corrupted region with high amplitude artifacts. The results show that overall the coherence values in delta and theta bands is high between the Raw and HAA data set. Furthermore, the coherence between Raw/HAA Data in *R1* is less than 0.5 in theta, alpha and beta bands. However, in spite of neighboring region R1, region R2 has very different results. Region *R2* presents results similar to regions *R3* and *R5*. Region *R5* is less corrupted with artifacts than regions *R2 and R3,* and because of this the main difference between the results is in delta band values, where the coherence is higher than 0.5 in regions *R2* and *R3* and over 0.5 in region *R5*. In the theta, alpha and beta bands the coherence value is similar in regions *R2*, *R3* and *R5*.

These results confirm that the selected components are mostly correlated to the delta bandwidth an ensure that the remaining frequency bands are unaffected, especially alpha and beta bands.

6. Event-Related Potentials

The aim of the current study was to show a new automatic selection algorithm for ICA decompositions to remove high amplitude artifacts in EEG signals. The data used in this study was highly corrupted with artifacts and hence compromises the interpretation of many psychophysiological correlates. In this particular case, the detection of ERP waves associated to performance in the HCT was nearly impossible. To show the impact of the application of this method and its ability to clean the high amplitude artifacts in the signal, the grand average signal of all participants in an average window between [200 - 300] *ms* after the feedback is used,which is depicted in Fig. 7(a). The grand average of the HAA and Clean Data in the same window is also considered, Fig. 7(b) and Fig. 7(c), respectively. The head topographies of the raw data show a high amplitude signal in the frontal channels that mask any ERP wave present.

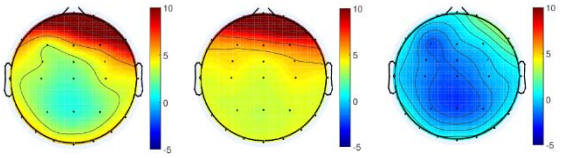

(a) (b) (c)

Fig. 7. Head topography of the grand average waveforms for all participants considering an average window between *[200 300] ms* after the feedback. (a) Raw Data; (b) HAA Data and (c) Clean Data.

After applying the SOBI algorithm and the automatic component selection, the Clean Data presents a negativity in the central area, that is not evident in the Raw data.

6.1. Feedback-related Negativity Wave

According to the neuroscience literature, the feedback-related negativity (FRN) is an ERP component maximally recorded in fronto-central areas of the scalp, which has been located to the Anterior Cingulate Cortex (ACC) [30].

In this work, all regions were processed but only region *R3* was chosen to be discussed, because the FRN effects were the strongest on it, in agreement with the existing literature. Fig. 8(a) displays the grand-average waveforms of individual ERPs for the region *R3* considering the two subsets of trials corresponding to the Right (ERPr) and Wrong (ERPw) answers, time-locked to the feedback. Thus, the value *0 ms* corresponds to the moment when the feedback occurred. In the displayed waveforms, we can observe large negative peaks after the feedback, peaking around *250 ms*, which are consistent with the feedback-related negativity. As can be observed, the FRN wave in the wrong subset (dash line) is more prominent than in the right subset (solid line). Furthermore, a difference between the Wrong and Right conditions is observed, with more negative amplitudes for the Wrong trials than for Righnt trials, Fig. 8(b), Fig. 8(c), respectively.

Note that the results obtained trial by trial with ICA are analogous to the results obtained considering the average signals [24]. In [24] a study with this HCT dataset is presented, where the goal was to characterize the ERPs associated to the HCT and simultaneously present a denoising technique.

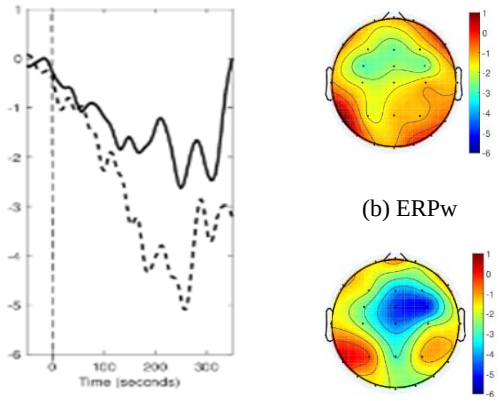

(a) FRN (b) ERPw (c) ERPr

Fig. 8. FRN analysis: (a) Grand-average waveforms of individual ERPs in region *R3* considering two subsets (ERPr and ERPw): Wrong response (dash line) and Right response (solid line). Head topography of the grand-average waveforms considering an average window between *[240 260] ms* after the feedback: (b) Wrong subset and (c) Right subset.

7. Conclusions

The aim of the component selection method described in this paper is to remove high amplitude

artifacts resulting from eye movements, patient movements, etc. It should be noted that this selection method is an advantageous alternative to those described in the literature as it is fully automatic and requires no input parameters to work. It is important to highlight the need to reduce the influence of high amplitude artifacts in EEG signals, not only to allow detection of ERP waves in neuroscience studies, but also for use of the EEG in BCI applications. Without doing so, one cannot be sure that the peaks observed in the signal reflect real brain processing and are not confounded with artifacts. After the preprocessing step, the data analysis revealed a frontocentral ERP wave related to error-processing: the feedback-related negativity (FRN), peaking around *250 ms* after feedback during performance on the HCT. As expected, errors elicited more negative amplitudes on that potential than correct responses [24].

Furthermore, results suggest that this error potential, the FRN, might provide an adequate method for detecting errors that requires no additional processing time and could thereby improve the speed and accuracy of EEG-based communication with devices using BCI applications. The use of Error Potentials in BCI applications arises from the observation that this additional information provided automatically by the user could be used to improve the BCI performance.

Acknowledgments

This work was supported by FCT grant (Ref: SFRH/BPD/101112/2014) to Ana Rita Teixeira and Bial Foundation grant (Ref: 136/08) to Isabel Santos.

References

[1]. L. F. Nicolas-Alonso, J. Gomez-Gil, Brain computer interfaces, a review, *Sensors (Basel)*, Vol. 12, No. 2, 2012, pp. 1211-1279.

[2]. L. Fernando Nicolas-Alonso, J. Gomez-Gil, Brain Computer Interfaces, a Review, *Sensors*, Vol. 12, No. 2, 2012, pp. 1211-1279.

[3]. A. Cichocki, Blind Signal Processing Methods for Analyzing Multichannel Brain Signals, *Int. J. Bioelectromagn.,* Vol. 6, No. 1, 2004, pp. 1-20.

[4] A. Kareem Abdullah, Z. Chao Zhu, Blind Source Separation Based of Brain Computer Interface System: A review, *Res. J. Appl. Sci. Eng. Technol.*, Vol. 7, No. 3, 2014, pp. 484-494.

[5]. Y. Chen, Q. Zhang, Y. Kinouchi, Blind Source Separation by ICA for EEG Multiple Sources Localization, in *Proceedings of the World Congress on Medical Physics and Biomedical Engineering 2006*, Berlin, Heidelberg, 2007, pp. 2760-2763.

[6]. H.-P. Huang, Y.-H. Liu, C.-P. Wang, T.-H. Huang, Automatic Artifact Removal in EEG Using Independent Component Analysis and One-Class Classification Strategy, *Journal of Neuroscience and Neuroengineering*, Vol. 2, No. 2, Apr. 2013, pp. 73-78.

[7]. M. Kirkove, C. François, J. Verly, Comparative evaluation of existing and new methods for correcting ocular artifacts in electroencephalographic recordings, *Signal Processing*, Vol. 98, May 2014, pp. 102-120.

[8]. A. K. Abdullah, C. Z. Zhang, A. A. A. Abdullah, S. Lian, Automatic Extraction System for Common Artifacts in EEG Signals Based on Evolutionary Stone's BSS Algorithm, *Math. Probl. Eng.*, Vol. 2014, Aug. 2014, pp. 1-25.

[9]. A. Delorme, T. Sejnowski, S. Makeig, Enhanced detection of artifacts in EEG data using higher-order statistics and independent component analysis, *Neuroimage*, Vol. 34, No. 4, Feb. 2007, pp. 1443-1449.

[10]. A. Mognon, J. Jovicich, L. Bruzzone, M. Buiatti, ADJUST: An automatic EEG artifact detector based on the joint use of spatial and temporal features, *Psychophysiology*, Vol. 48, No. 2, Feb. 2011, pp. 229-240.

[11]. H. Nolan, R. Whelan, R. B. Reilly, FASTER: Fully Automated Statistical Thresholding for EEG artifact Rejection, *J. Neurosci. Methods*, Vol. 192, No. 1, Sep. 2010, pp. 152-162.

[12]. M. Chaumon, D. V. M. Bishop, N. A. Busch, A practical guide to the selection of independent components of the electroencephalogram for artifact correction, *J. Neurosci. Methods*, Vol. 250, Mar. 2015, pp. 47-63.

[13]. L. Albera, A. Kachenoura, P. Comon, A. Karfoul, F. Wendling, L. Senhadji, I. Merlet, ICA-Based EEG denoising: a comparative analysis of fifteen methods, *Bull. Polish Acad. Sci. Tech. Sci.*, Vol. 60, No. 3, Jan. 2012, pp. 407-418.

[14]. H. Zeng, A. Song, R. Yan, H. Qin, EOG Artifact Correction from EEG Recording Using Stationary Subspace Analysis and Empirical Mode Decomposition, *Sensors*, Vol. 13, No. 11, Nov. 2013, pp. 14839-14859.

[15]. P. Mishra, S. K. Singla, Artifact Removal from Biosignal using Fixed Point ICA Algorithm for Pre-processing in Biometric Recognition, *Meas. Sci. Rev.*, Vol. 13, No. 1, 2013.

[16]. I. Daly, M. Billinger, R. Scherer, G. Muller-Putz, On the automated removal of artifacts related to head movement from the EEG, *IEEE Trans. Neural Syst. Rehabil. Eng.*, Vol. 21, No. 3, May 2013, pp. 427-434.

[17]. W. Kong, Z. Zhou, S. Hu, J. Zhang, F. Babiloni, G. Dai, Automatic and direct identification of blink components from scalp EEG, *Sensors (Basel)*, Vol. 13, No. 8, Jan. 2013, pp. 10783-10801.

[18]. M. Silvetti, E. Nuñez Castellar, C. Roger, T. Verguts, Reward expectation and prediction error in human medial frontal cortex: an EEG study, *Neuroimage*, Vol. 84, Jan. 2014, pp. 376-382.

[19]. A. R. Teixeira, A. M. Tomé, I. M. Santos, Automatic Elimination of High Amplitude Artifacts in EEG Signals, in *Proceedings of the First International Conference on Advances in Signal, Image and Video Processing (SIGNAL'16)*, 2016, pp. 21-26.

[20]. P. W. Ferrez, J. del R Millan, Error-related EEG potentials generated during simulated brain-computer interaction, *IEEE Trans. Biomed. Eng.*, Vol. 55, No. 3, Mar. 2008, pp. 923-929.

[21]. I. Iturrate, L. Montesano, J. Minguez, Task-dependent signal variations in EEG error-related potentials for brain–computer interfaces, *J. Neural Eng.*, Vol. 10, No. 2, Apr. 2013, p. 026024.

[22]. M. Falkenstein, J. Hoormann, S. Christ, J. Hohnsbein, ERP components on reaction errors and

their functional significance: A tutorial, *Biol. Psychol.*, Vol. 51, No. 2-3, 2000, pp. 87-107.
[23]. T. U. Hauser, R. Iannaccone, P. Stämpfli, R. Drechsler, D. Brandeis, S. Walitza, S. Brem, The feedback-related negativity (FRN) revisited: new insights into the localization, meaning and network organization, *Neuroimage*, Vol. 84, Jan. 2014, pp. 159-168.
[24]. I. M. Santos, A. R. Teixeira, A. M. Tomé, A. T. Pereira, P. Rodrigues, P. Vagos, J. Costa, M. L. Carrito, B. Oliveira, N. A. DeFilippis, C. F. Silva, ERP correlates of error processing during performance on the Halstead Category Test, *Int. J. Psychophysiol*, Vol. 106, 2016, pp. 97-105.
[25]. I. Daly, N. Nicolaou, S. J. Nasuto, K. Warwick, Automated artifact removal from the electroencephalogram: a comparative study, *Clin. EEG Neurosci*, Vol. 44, No. 4, Oct. 2013, pp. 291-306.
[26]. A. M. Tome, E. W. Lang, Approximate diagonalization approach to blind source separation with a subset of matrices, in *Proceedings of the Seventh International Symposium on Signal Processing and Its Applications,* Vol. 2, 2003, pp. 105-108.
[27]. A. Cichocki, S. Amari, Adaptive Blind Signal and Image Processing: Learning Algorithms and Applications, *John Wiley & Sons*, *Ltd*, 2002.
[28]. J. P. Choca, L. Laatsch, L. Wetzel, A. Agresti, The Halstead Category Test: a fifty year perspective, *Neuropsychol. Rev.*, Vol. 7, No. 2, 1997, pp. 61-75.
[29]. P. Stoica, R. Moses, Spectral Analysis of Signals, *Prentice Hall,* Upper Saddle River, New Jersey, 2004.
[30]. W. H. R. Miltner, C. H. Braun, M. G. H. Coles, Event-related brain potentials following incorrect feedback in a time-estimation task: Evidence for a generic neural system for error detection, *Journal of Cognitive Neuroscience*, Vol. 9, No. 6, 1997, pp. 788-798.